Nanoscale

COMMUNICATION

View Article Online
View Journal | View Issue

Cite this: *Nanoscale*, 2025, **17**, 25003

Received 11th April 2025,
Accepted 16th October 2025

DOI: 10.1039/d5nr01468a

rsc.li/nanoscale

Beating-wave analysis of small-angle X-ray scattering of unilamellar liposomes loaded with model drug Benzocaine

Laura Baraldi, *†[a] Serena R. Alfarano,[b] Flávia Sousa, ‡[a] Luciano Marchiò, [c] Alessia Bacchi, [c] Raffaele Mezzenga, [b] Barbara Rothen-Rutishauser, [a] Alke Petri-Fink [a] and Sandor Balog *[a]

A robust mathematical model was developed to characterize the liposomal bilayer *via* small-angle X-ray scattering (SAXS). The model was tested on four liposome formulations having the same excipients but different loaded drugs, demonstrating high accuracy in drawing the electron density profiles, highlighting their differences.

The COVID pandemic has taught us that we might face other devastating and rapidly spreading infectious diseases in the future due to increasing population, worldwide commerce, globetrotting, sedentary lifestyle, massive consumption of meat, microplastics in the environment, and waterborne diseases resulting from global warming.[1] Consequently, academic research and pharmaceutical R&D must be even faster in responding to unforeseen scenarios. These days, nearly 600 liposomal formulations are in ongoing clinical trials,[2] and ensuring quality in production scalability[3] and characterization[4] are significant bottlenecks. In other words, developing a successful formulation not only requires synthetic excellence but efficient purification and accurate characterization.[5]

Liposomes are the first generation of lipid nanoparticles (LNP). Since their discovery in 1965,[6] liposomes (*i.e.*, phosphatidylcholine lipid vesicles) have been used to deliver drugs, such as small molecules and nucleic acids,[7] as biocompatible formulations.[8] They comprise an aqueous core and one or more hydrophobic shells composed of a head–tail–tail–head phospholipid bilayer. This structural arrangement can encapsulate hydrophilic and lipophilic drugs and drugs at the interface between the aqueous core and the bilayer.[9] Their popularity arises from the ability to protect the drug from degradation and effectively deliver it where needed, thus reducing side effects.[10] Over the years, much progress has been made in developing liposomal formulations: many targets have been reached, addressing different pathologies—such as cancer, pain, and infections—by tailoring the composition and functionalizing the surface of the liposomes.[11] For instance, ionizable cationic lipids can be enrolled to interact with labile solutes like mRNA and then actively trigger their release inside the cell.[12] This formulation strategy saved many lives during the COVID pandemic, where the mRNA coding for the coronavirus spike protein was entrapped into lipid-based colloidal particles to produce vaccines.[13] Like most colloidal soft matter, liposomes are dynamic systems[14,15] sensitive to external stimuli.[16] Accordingly, liposomes must be characterized in their native state, under ambient conditions, *in situ*, and in a non-invasive and non-destructive manner. Particle size and size distribution may be readily characterized *via*, *e.g.*, dynamic and static light scattering.[14] Characterizing the structural features of the membrane-like lipid bilayer, however, requires sub-nanometer resolution and high statistical power,[15] and small-angle X-ray scattering (SAXS) is the first-choice experimental technique.[17]

SAXS provides quantifiable information on the nanoscale structure and morphology on the length-scale of roughly 1–100 nm of the sample studied. SAXS is a conceptually simple technique:[18] the dispersion of the lipid particles is irradiated with a narrow and collimated beam of quasi-monochromatic soft X-rays—photon wavelength is roughly between 0.1–10 nm—which interacts quasi-elastically with the dispersion. The X-rays scattered off the particles are detected with a position-sensitive area detector. The intensity of scattering as a function of the scattering angle (referred to as scattering pattern) is a function of the volumetric distribution of the electrons (referred to as electron

[a]*Adolphe Merkle Institute and National Center of Competence in Research Bio-Inspired Materials, University of Fribourg, Chemin des Verdiers 4, 1700 Fribourg, Switzerland. E-mail: sandor.balog@unifr.ch, laura.baraldi@hest.ethz.ch*
[b]*Department of Health Sciences and Technology, ETH Zürich, Zürich 8092, Switzerland*
[c]*Department of Chemistry, Life Sciences and Environmental Sustainability, University of Parma, 43124 Parma, Italy*
†Present Address: Laura Baraldi - Department of Health Sciences and Technology, ETH Zürich, Zürich 8092, Switzerland.
‡Present Address: Flávia Sousa – Department of Pharmaceutical Technology and Biopharmacy, University of Groningen, 9713 AV Groningen, The Netherlands.

density) within the atomic and molecular bricks making up the lipid formulation. Thus, the scattering pattern is characteristic of the atomic and molecular arrangement of matter on the nanoscale, and thus, it carries information about the orientation, shape, and size of domains.

From a mathematical perspective, the recorded scattering pattern is proportional to the square of the Fourier transform of the electron density distribution $\rho(\vec{r})$ in the material, $I(\vec{q}) \propto |\mathrm{FT}\rho(\vec{r})|^2$, and thus, by analyzing the SAXS profile, information on the nanoscale structure and morphology of the sample studied may be quantified. In case of liposomes, $|\mathrm{FT}\rho(\vec{r})|^2$ may be referred to as the form factor: $P(\vec{q}) = |\mathrm{FT}\rho(\vec{r})|^2$. The angular dependence is defined through the so-called scattering vector, whose amplitude is $q = 4\pi/\lambda \sin\theta/2$, where θ is the scattering angle and λ the wavelength.

Fig. 1 shows an idealized structural sketch of a spherical lipid membrane. Phospholipids are a class of lipids made of three main structural components: a polar head group, a nonpolar tail, and a glycerol backbone. The polar head is hydrophilic, while the nonpolar tail is hydrophobic. The backbone connects the head and the tail. The electron densities of these components are different, and therefore SAXS may be used to study how lipids are assembled. In an aqueous environment, liposomes exhibit a relatively well-defined membrane-like shell: the head groups face towards the aqueous environment, both inside and outside, and the tails are oriented inwards. According to this view, one may define a tangential and a radial electron density profile. Given that the interest lays mostly in characterizing the bilayer thickness, most of the time it is implicitly assumed that the tangential profile is constant, which may be an adequate approximation, but not strictly correct. Nonetheless, while the lipids are indeed discrete units, their spherical assembly shows a high-degree n-fold rotational symmetry ($n \gg 1$) that may be approximated as being quasi-isotropic. This assumption greatly simplifies the Fourier transform of the electron density of the lipid bilayer, which is essentially an integral over the scattering volume:

$$\mathrm{FT}(\vec{r}) = 4\pi \int \rho(r) \cdot \frac{\sin(q \cdot r)}{q \cdot r} r^2 \mathrm{d}r \tag{1}$$

where $\rho(r)$ is an isotropic radial function that embodies the electron density profile of the structure across the bilayer.

Seminal works—using X-rays and showing for the first time that lipid membranes feature a bilayer that may interact with, *e.g.*, proteins—were carried out early in the 70s.[19] The nanoscale radial structure was found to exhibit a systematic variation in the electron density profile across the membrane, which consist of two peaks separated by a broad dip, originating from the difference between the electron density of the lipids and the one of the water buffer. The first feature is attributed to the head groups, composed of P/O/N atoms, having (on average) a higher electron density than those of the buffer solvent, while the dip indicated the fatty chains with low electron density (comprising only C/H atoms, having a lower electron density than those of the buffer). This structural view still defines the current mainstream in the analysis of SAXS spectra,[20,21] where, $\rho(r)$ is most frequently modeled by the sum of at least three Gaussian functions (Fig. 1a): two for the polar heads, and one for the tails and backbone

$$\rho(r) = \sum_{i=1}^{3} \rho_i(r) \tag{2}$$

where $\rho_i(r)$ stands for a regular Gaussian function with a mean μ_i, variance σ_i^2, and amplitude a_i

$$\rho_i(r) = a_i \frac{\mathrm{e}^{-\frac{(r-\mu_i)^2}{2\sigma_i^2}}}{\sqrt{2\pi}\sigma_i} \tag{3}$$

Integration in eqn (1) is a linear operation, and therefore eqn (2) may be evaluated as

$$\mathrm{FT}\sum_{i=1}^{3} \rho_i(r) = \sum_{i=1}^{3} \mathrm{FT}\rho_i(r) \tag{4}$$

Evaluating the Fourier transform of a Gaussian function yields a closed form expression[20]

$$\mathrm{FT}\rho_i(r) = A_i(f_i + g_i) \tag{5}$$

where $A_i = 4\pi \cdot a_i \cdot e^{-\frac{1}{2}q^2\sigma_i^2}$, $f_i = \sin(\mu_i \cdot q)\frac{\mu_i}{q}$, $g_i = \cos(\mu_i \cdot q) \cdot \sigma_i^2$. With this, one can now express the form factor:

$$\mathrm{FT}\,\delta(r) = \sum_{i=1}^{3} \mathrm{FT}\,\delta_i(r) = \sum_{i=1}^{3} A_i(f_i + g_i) \tag{6}$$

and

$$P(q) = \left| \sum_{i=1}^{3} A_i(f_i + g_i) \right|^2 \tag{7}$$

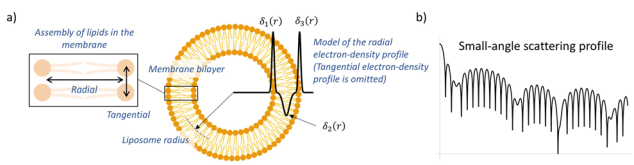

Fig. 1 (a) Illustration of the cross-sectional structure of spherical and symmetric lipid membranes. Such spherical and uni-lamellar assembly exhibits two main symmetries: one in the radial direction, and the other in the tangential direction, as indicated by the arrows. The tangential profile represents circular/spherical stacking of lipids, which is usually omitted in SAXS analysis of membrane thickness. This work, as most works, addresses the radial profile. The solid line—drawn as the sum of three Gaussian functions— $\delta(r) = \sum_{i=1}^{3} \delta_i(r)$, two for the heads and one for tails of the lipids—shows a plausible mathematical model of the radial profile of the bilayer electron density. (b) Scattering profile: the square of the Fourier Transform of the radial profile contains quantitative information about the membrane structure and is directly measurable *via* SAXS.

Eqn (7) operates only on real-valued numbers, and by using the properties of the absolute value function we rewrite eqn (7):

$$P(q) = \left(\sum_{i=1}^{3} A_i(f_i + g_i)\right)^2. \quad (8)$$

What remains is accounting for the fact that liposomes exhibit size polydispersity, which necessitates an additional integration of eqn (8) over the distribution of liposome radius:

$$P(q) = \int p(r)P(q,r)\mathrm{d}r. \quad (9)$$

Eqn (9) does not yield a closed-form analytical solution but may be evaluated numerically. Describing the size distribution $p(r)$ involves at least two additional parameters: mean radius and standard deviation of the radius. Accordingly, if the bilayer is not symmetric, one has 11 parameters in total. Nonetheless, this parametric model is conceptually very elegant, and the so-called forward problem, that is, predicting the SAXS spectrum from a given electron-density radial function of liposomes, is straightforward *via* eqn (1)–(9). Fig. 2 shows a representative set of simulated scattering spectra of two symmetric bilayers with systematically varied radius. The liposome radius is defined at the global minimum of the radial profile (Fig. 1a). One may identify two dominant features in the SAXS spectra: the first, is a rapid oscillatory function that is modulated by a second and slowly varying envelope function. The rapid oscillations (Fig. 2b) relate to particle radius and vanish upon size polydispersity (Fig. 2c). With polydispersity, the scattering spectra approaches the envelope of the form factor, indicating that the SAXS spectrum contains more features resulting from the radial profile compared to the size of the liposome.

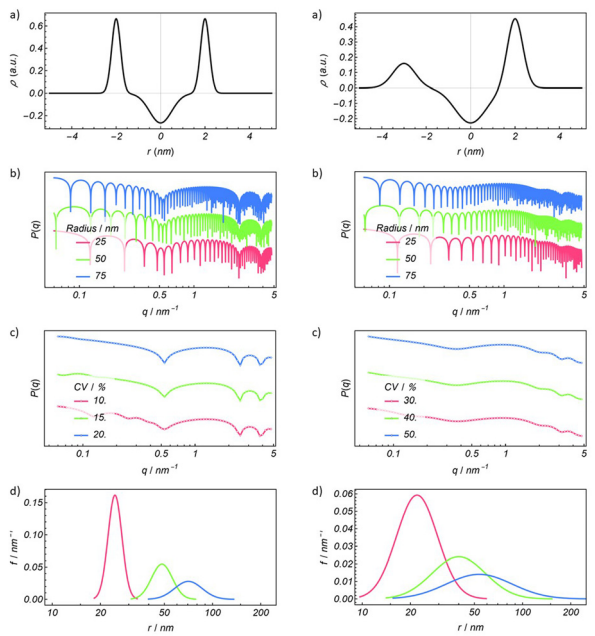

Fig. 2 Scattering spectra computed *via* eqn (1)–(9). (a) Simulation of two arbitrary symmetric radial profiles of liposomes, a symmetric and an asymmetric one, and (b) the corresponding scattering spectra with different radii. While the spectra are seemingly complex, one may identify two dominant features: (1) a rapid oscillatory function that is modulated by (2) a slowly varying envelope function. (c) The rapid oscillations, which are related to particle radius, vanish upon increasing polydispersity in the radius, and the scattering spectra approaches the envelope of the form factor. CV, the coefficient of variation, is defined as the ratio of the standard deviation and the mean. (d) Corresponding lognormal distributions of the radius modelling polydispersity.

Doing this transformation backward, which is referred to as the inverse problem, is much more difficult, and a solution usually requires deep domain-specific knowledge. Given that the model may be amenable to parametric analysis, most of the time, $\rho(r)$ is modeled explicitly, and the model evaluated and regressed against experimental SAXS spectra. In this way, one can infer the model's parameters, and thus characterize the structure of the studied bilayer. However, even the simplest Gaussian model comes with nine parameters: three amplitudes, three centers, and three widths. In the case of symmetric membranes, nine reduces to six since the outer Gaussian parameters would be equal to the inner Gaussian parameters. If size polydispersity is considered, the number of regression parameters increases according to the complexity of the size distribution. Commercial and free computational tools dedicated to the analysis of small-angle scattering spectra have been made available,[22] yet the mathematical apparatus, both analytical and numerical, might be well beyond the expertise of most scientist concerned with the development of novel lipid formulations. Indeed, in our experience, obtaining a physically meaningful and converging solution of the inverse problem has been proven to be highly uncertain, and by using freely available computational tools, we failed to analyze even well-defined idealized synthetic spectra. Thus, we believe there is a dire need of an accessible and reliable tool to analyze SAXS spectra of lipid membrane bilayers.

Here we set out to develop a simple yet useful alternative. We focus on two aspects: (1) we aim at an approach that considerably decreases the complexity of the analysis, yet (2) it infers the features of the parametric model of the membrane electron-density profile with a good statistical accuracy. For this, we will focus on deriving and utilizing the envelope function. This envelop function is not an exact solution, but it is a good approximation considering the practical limitations—such as noise, dynamic range (q-range), and resolution—of most SAXS data recorded on lab-scale instruments. The fact that SAXS spectra are rather insensitive to the size and polydispersity of liposomes, and the structural information about the bilayer profile is carried only by the envelope of the spectra (Fig. 2b and c) was pointed-out already in 1975,[23] yet, to the best of our knowledge, the relevance in the SAXS analysis of liposomes has never been recognized nor deployed. We show here that this approach is both straightforward and beneficial.

Eqn (3) describes the Gaussian models of the radial profile, and eqn (8) describes the form factor. The radius and the thickness of the membrane of the application-relevant liposomes are such that $\mu_i/q \gg \sigma_i^2$, over the q-range of the SAXS

spectra.[20] As a consequence, $f_i \gg g_i$, and one can truncate the expression: $f_i + g_i \cong f_i$. Thus, eqn (5) and (8) simplify: FT $\delta_i(r) \cong A_i f_i$, and we may write:

$$P(q) \cong \left(\sum_{i=1}^{3} A_i f_i\right)^2. \quad (10)$$

A simple computational series (similarly to Fig. 2) proved that omitting the term g_i will not change the observable spectra, as the difference resulting from having or not having the term g_i in the form factor is well below the noise-level of experimental spectra. Now, the truncated version of the from factor (eqn (10)) encourages us to look at the form factor from another angle and consider it as the amplitude of the linear superposition of three harmonic waves. After all, SAXS essentially relies on a well-known wave phenomenon: interference of coherent waves. An important aspect to recognize is the fact that the membranes of such liposomes are thin, that is, $|\mu_i - \mu_j| \ll \mu_i$. In other words, the frequencies of the harmonic waves are very close to one another. This proximity of spatial frequencies, and the superposition of harmonic waves having slightly different frequencies results in a special wave phenomenon: beating waves (Fig. 3).[24]

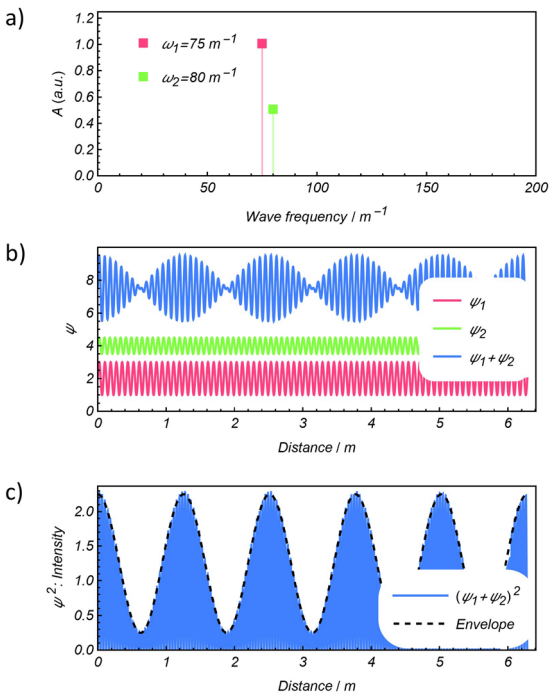

Fig. 3 Beating of two superposing harmonic waves. (a) The frequency and amplitudes of two harmonic waves, and (b) their waveform: $\Psi_i = A_i \cdot \sin(\omega_i \cdot x)$. (The waveforms are shifted vertically for the sake of visibility.) The linear superposition of the waves with slightly different frequencies form beats, which appear as a slow harmonic modulation of the amplitude of the rapid oscillations. The frequency of this modulation (the beat frequency) is solely defined by the difference of the two frequencies: $\omega_B = |\omega_1 - \omega_2|$. (c) The intensity of the superposing waves is covered by an envelope function: $f_E(x) = A_1^2 + A_2^2 + 2A_1A_2 \cdot \cos(\omega_i \cdot x)$.

In fact, what we can observe in Fig. 2b is the same wave-beating phenomena resulting from the superposition of three waves: $\sum_{i=1}^{3} A_i f_i$, where the envelope function is the intensity beats of the three superposing waves. It is easy to show that for N harmonic waves with amplitudes A_i and frequency ω_i, the envelope function is given by:

$$f_E(x) = \sum_{i=1}^{N} A_i^2 + 2\sum_{i=1}^{N-1}\sum_{j>i}^{N} A_i A_j \cdot \cos(\omega_{ij} \cdot x) \quad (11)$$

where the respective beat frequencies are $\omega_{ij} = |\omega_i - \omega_j|$. In our case, we can now apply eqn (11) to describe the SAXS spectra of liposome membranes, where according to the Gaussian model, each wave is composed of an amplitude and a harmonic term with frequency μ_i:

$$4\pi \cdot a_i \cdot e^{-\frac{1}{2}q^2\sigma_i^2} \mu_i/q \times \sin(\mu_i \cdot q). \quad (12)$$

Using eqn (11) and (12), eqn (10) is easily evaluated and provides a simple and symmetric closed form for the analysis of SAXS spectra on liposomes:

$$\begin{aligned} P(q) = {} & \frac{1}{q^2}\sum_{i=1}^{3} a_i^2 \cdot \mu_i^2 \cdot e^{-q^2\sigma_i^2} \\ & + \frac{1}{q^2}\Big(2a_1a_2\mu_1\mu_2 e^{\frac{1}{2}q^2(\sigma_1^2+\sigma_2^2)} \cos(q(\mu_2-\mu_1)) \\ & + 2a_1a_3\mu_1\mu_3 e^{\frac{1}{2}q^2(\sigma_1^2+\sigma_3^2)} \cos(q(\mu_3-\mu_1)) \\ & + 2a_2a_3\mu_3\mu_3 e^{\frac{1}{2}q^2(\sigma_2^2+\sigma_3^2)} \cos(q(\mu_3-\mu_3))\Big) \end{aligned} \quad (13)$$

Our model does not assume or impose any symmetry or asymmetry in the bilayer structure, and the model therefore accommodates arbitrary bilayer configurations without constraint.

As a proof of concept for the beating-wave model, we synthesized four liposome formulations loaded with drug (benzocaine salts) and collected SAXS spectra (see SI). The excipient components and the preparation process were identical for every sample, with the only difference being the loaded drug (see SI). Specifically, one liposome formulation was empty (Lipo Placebo), one was loaded with benzocaine (Lipo Benzocaine), and the other two contained two different benzocaine salts. Among the newly synthesized benzocaine systems reported in our previous work,[25] benzocaine maleate and benzocaine camphorsulfonate were encapsulated within liposome formulations (Lipo Benzocaine Camphorsulfonate and Lipo Benzocaine Maleate), which were then compared to the placebo and the liposome loaded with benzocaine alone.

Eqn (13) was used to fit the experimental SAXS spectra, *via* nonlinear ordinary least-squares regression. All symbolic and numerical evaluations of the model and its parts were obtained by using Mathematica (Version 13.0, Wolfram Language, Wolfram Research, Inc., Champaign, IL). The aim was to find and identify potentially different interactions between the drugs, having slightly different physicochemical properties, and the liposome shell, as manifesting in the electron density profile. In Fig. 4, we present the raw data (colored symbols) with the curves of the best-fitting models (black line).

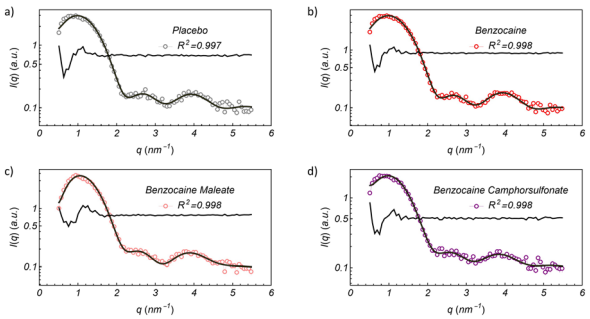

Fig. 4 SAXS spectra of four liposomal formulations: (a) Placebo (grey), (b) Benzocaine (red), (c) Benzocaine Maleate (pink), (d) Benzocaine Camphorsulfonate (purple). The solid lines are the regressions (eqn (13)) and the corresponding residuals of the model (vertically shifted for visibility). The coefficient of determination is indicated in each panel.

The regressions are of good quality, follow closely the experimental data. The SAXS features of liposomes are evident, characterized by the presence of discernible harmonic peaks. We can observe slight variations, particularly between Lipo Benzocaine Maleate and the other samples, with the second scattering peak slightly shifted to the left compared to the rest. Fig. 5 shows the corresponding bilayer's profile as expressed in radial distance (unit: nm) by the electron density difference (contrast) relative to the mean value (ρ). The radial profiles reveal subtle distinctions among the samples: a noticeable contrast emerges in the central region (Fig. 5), suggesting the localization of benzocaine between the lipid tails, as evidenced by the heightened contrast in the central Gaussian corresponding to the tail–tail segment of the bilayer. Indeed, after encapsulating a hydrophobic molecule within the lipid bilayer, a subsequent disruption of the phospholipid's arrangement might occur. Hence, the change in the contrast. Additionally, the electron density profile indicates an expansion of the bilayer in the Lipo Benzocaine Maleate formulation, witnessed by the larger distance between the beginning of the inward head Gaussian and the end of the outward head Gaussian (from 5.7 nm in Lipo Placebo and Lipo Benzocaine to 6.4 nm in Lipo Benzocaine Maleate). This increase suggests a change in the bilayer structure attributable to the altered physiochemical properties of benzocaine maleate compared to benzocaine

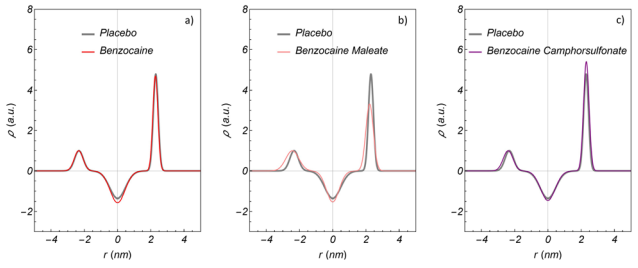

Fig. 5 Electron density contrast profile of the bilayer of different liposomal formulations superimposed with the placebo (grey): (a) Benzocaine (red), (b) Benzocaine Maleate (pink), (c) Benzocaine Camphorsulfonate (purple).

alone, guaranteeing the encapsulation of the salt. This different structural organization could hypothetically lead to an ameliorated *in vivo* release, providing a desired synergy between crystal engineering and formulation engineering. In contrast, Lipo Benzocaine Camphorsulfonate shows only minor differences compared to the placebo liposomes, possibly due to the lower stability of the salt throughout the liposome production process (see Fig. 5).

Our electron density profiles show that the bilayers are not symmetric, particularly in the Lipo Benzocaine Maleate formulation, which induces bilayer expansion. This asymmetry may result from differential leaflet packing, drug insertion depth, or curvature stress. Electron density contrast profiles of lipid bilayers provide insight into the molecular structure across the membrane, revealing regions of high and low electron density that correspond to lipid headgroups and hydrophobic tails, respectively. These profiles also show how water interacts with the bilayer, with gradual transitions at the edges indicating hydration and mixing. Asymmetry in the profile suggests structural differences between the two leaflets, which may arise from uneven lipid distribution or interactions with the surrounding solution. A likely cause of this asymmetry is the preferential localisation of DSPE-PEG on the outer leaflet due to its bulky, hydrophilic PEG chains, resulting in higher electron density on one side. Additionally, differences in the composition of the internal vesicle pool compared to the external solution could influence the inner leaflet's profile, especially through interfacial mixing or solute adsorption. These factors together shape the bilayer's structural and functional properties, and changes in environmental conditions can further modulate the profile, revealing dynamic membrane behaviour. However, we did not investigate these aspects in detail. Our focus was on the verification and validation of our new mathematical model.

Furthermore, the lower encapsulation efficiency (EE%) of the maleate salt compared to camphorsulfonate likely stems from the maleate's higher polarity and stronger hydration, which reduces its affinity for the lipid bilayer. In contrast, the more hydrophobic camphorsulfonate counterion favours bilayer partitioning, resulting in higher EE%. Interestingly, despite its lower EE%, the maleate salt induces the most pronounced perturbation in the bilayer electron density profile. This suggests that even small amounts of incorporated maleate interact strongly with lipid headgroups, significantly affecting bilayer organisation.

Conclusions

We introduced a valuable alternative, based on the phenomenon of beating waves, in the SAXS analysis of liposomes. This parametric model affords a direct nonlinear regression with a minimal number of parameters and provides an estimate of the electron-density profile of the bilayer model. We addressed the challenge most often encountered in SAXS analysis: being accessible and applicable to a broader range of scientists working on lipid formulations.

We demonstrated the new model on liposomes loaded with benzocaine salts: the model showed that benzocaine localized between lipid tails, which can induce an expansion of the bilayer host. The structural variations between the placebo and drug-loaded samples were significantly larger than the experimental variability and uncertainty corresponding to the placebo formulation, and therefore, the observed differences in electron density profiles may be attributed to the presence and partitioning of the guest compounds.

The relative dimensions between the bilayer and the vesicle shell are key to interpreting SAXS data accurately. When the bilayer's structural features are much smaller than the vesicle radius, their scattering signals (*i.e.*, form factors) remain distinct and do not interfere. A minimum vesicle radius is required to maintain bilayer integrity, as high curvature introduces mechanical stress. This becomes critical when the radius-to-thickness ratio drops below ten, and vesicles smaller than ~20 nm may transition into micellar or bicellar forms. Additionally, typical SAXS q-ranges are often too low to resolve vesicle sizes around 100 nm, limiting direct observation of size-related features.

Regarding experimental noise, any scattering technique is essentially a mathematical inverse problem, and our resolution and bias are strictly noise-limited. Therefore, the better the data in terms of noise, the more reliable (in terms of accuracy and precision) the regression analysis. Therefore, while SAXS provides unique and quick *in situ* access to the bilayer electron density profile, complementary methods such as cryo-TEM, fluorescence microscopy, DSC may further corroborate structural information obtained by X-ray scattering.

Finally, a Mathematica (Wolfram Language) implementation of the model, along with usage instructions, is freely available from the authors upon request.

Author contributions

Project administration, A. P–F., S. B., L. B., B. R-R., R. M., L. M., A. B.; sample preparation, L. B., F. S.; data collection, S. R. A., L. B.; mathematical modeling and data analysis, S. B.; all authors have read and agreed to the published version of the manuscript.

Conflicts of interest

There are no conflicts to declare.

Data availability

The data supporting this article have been included as part of the supplementary information (SI). Supplementary information is available. The Supplementary Information file includes detailed descriptions of the materials, methods, and characterization techniques used throughout the study. See DOI: https://doi.org/10.1039/d5nr01468a.

Acknowledgements

The University of Parma, Italy, the Adolphe Merkle Foundation and the University of Fribourg, Switzerland financially supported this work. This work also benefitted from support of the Swiss National Science Foundation through the National Center of Competence in Research Bio-Inspired Materials.

References

1 A. M. Edwards, R. S. Baric, E. O. Saphire and J. B. Ulmer, *Science*, 2022, **375**, 1133–1139.
2 ClinicalTrials.gov. https://beta.clinicaltrials.gov/.
3 L. M. Liz-Marzán, A. E. Nel, C. J. Brinker, W. C. W. Chan, C. Chen, X. Chen, D. Ho, T. Hu, K. Kataoka, N. A. Kotov, W. J. Parak and M. M. Stevens, *ACS Nano*, 2022, **16**, 13257–13259.
4 Y. Fan, M. Marioli and K. Zhang, *J. Pharm. Biomed. Anal.*, 2021, **192**, 113642.
5 N. Dimov, E. Kastner, M. Hussain, Y. Perrie and N. Szita, *Sci. Rep.*, 2017, **7**, 12045.
6 A. D. Bangham, M. M. Standish and J. C. Watkins, *J. Mol. Biol.*, 1965, **13**, 238–252.
7 R. Tenchov, R. Bird, A. E. Curtze and Q. Zhou, *ACS Nano*, 2021, **15**, 16982–17015.
8 G. Gregoriadis and B. E. Ryman, *Eur. J. Biochem.*, 1972, **24**, 485–491.
9 D. E. Large, R. G. Abdelmessih, E. A. Fink and D. T. Auguste, *Adv. Drug Delivery Rev.*, 2021, **176**, 113851.
10 A. Sesarman, D. Muntean, B. Abrudan, L. Tefas, B. Sylvester, E. Licarete, V. Rauca, L. Luput, L. Patras, M. Banciu, L. Vlase and A. Porfire, *J. Liposome Res.*, 2021, **31**, 1–10.
11 M. Kapoor, S. L. Lee and K. M. Tyner, *AAPS J.*, 2017, **19**, 632–641.
12 G. Lou, G. Anderluzzi, S. T. Schmidt, S. Woods, S. Gallorini, M. Brazzoli, F. Giusti, I. Ferlenghi, R. N. Johnson, C. W. Roberts, D. T. O'Hagan, B. C. Baudner and Y. Perrie, *J. Controlled Release*, 2020, **325**, 370–379.
13 G. Gregoriadis, *Med. Drug Discovery*, 2021, **12**, 100104.
14 M. Danaei, M. Dehghankhold, S. Ataei, F. Hasanzadeh Davarani, R. Javanmard, A. Dokhani, S. Khorasani and M. R. Mozafari, *Pharmaceutics*, 2018, **10**, 57.
15 F. A. Heberle and G. Pabst, *Biophys. Rev.*, 2017, **9**, 353–373.
16 T. R. S. Prakash and K. Soni, *Pharm. Nanotechnol.*, 2021, **9**, 347–360.
17 Y. Da Dong and B. J. Boyd, *Int. J. Pharm.*, 2011, **417**, 101–111.
18 T. Li, A. J. Senesi and B. Lee, *Chem. Rev.*, 2016, **116**, 11128–11180.
19 Y. K. Levine and M. H. F. Wilkins, *Nat. New Biol.*, 1971, **230**, 69–72.
20 M. R. Brzustowicz and A. T. Brunger, *J. Appl. Crystallogr.*, 2005, **38**, 126–131.

21 J. A. Bouwstra, G. S. Gooris, W. Bras and H. Talsma, *Chem. Phys. Lipids*, 1993, **64**, 83–98.
22 J. Ilavsky and P. R. Jemian, *J. Appl. Crystallogr.*, 2009, **42**, 347–353.
23 M. F. Moody, *Acta Crystallogr., Sect. A*, 1975, **31**, 8–15.
24 H. A. Radi and L. O. Rasmussen, in *Principles of Physics: For Scientists and Engineers*, 1975, 8–15.
25 L. Baraldi, I. Bassanetti, F. Amadei, A. Bacchi and L. Marchiò, *Cryst. Growth Des.*, 2024, **24**, 2157–2167.